Am J Cancer Res 2024;14(3):1015-1032
www.ajcr.us /ISSN:2156-6976/ajcr0155139

Original Article

Inactivation of ERK1/2 in cancer-associated hepatic stellate cells suppresses cancer-stromal interaction by regulating extracellular matrix in fibrosis

Qirui Lin[1,2], Defeng Lei[1], Tongning Zhong[3], Yanmin Zhang[3], Qingen Da[4], Xiao Chen[1], Xuemei Li[5], Jikui Liu[1], Zilong Yan[1]

[1]Department of Hepatobiliary Surgery, Peking University Shenzhen Hospital, Shenzhen 518000, Guangdong, China; [2]Department of Clinical Application, Center for iPS Cell Research and Application (CiRA), Kyoto University, Kyoto 6068507, Japan; [3]Central Laboratory, Peking University Shenzhen Hospital, Shenzhen 518000, Guangdong, China; [4]Department of Cardiovascular Surgery, Peking University Shenzhen Hospital, Shenzhen 518000, Guangdong, China; [5]Department of Gynecology, Zhanjiang Maternity and Child Healthcare Hospital, Zhanjiang 524000, Guangdong, China

Received December 27, 2023; Accepted March 7, 2024; Epub March 15, 2024; Published March 30, 2024

Abstract: The ERK1/2 pathway is involved in epithelial-mesenchymal transformation and cell cycle of tumor cells in hepatocellular carcinoma (HCC). In the present study, we investigated the involvement of ERK1/2 activation on hepatic stellate cells (HSCs). We identified ERK1/2 phosphorylation in activated HSCs of HCC samples. We found that tumor cells promoted the migration and invasion capacity of HSCs by activating ERK1/2 phosphorylation. Using high throughput transcriptome sequencing analysis, we found that ERK1/2 inhibition altered genes significantly correlated to signaling pathways involved in extracellular matrix remodeling. We screened genes and demonstrated that the ERK1/2 inhibition-related gene set significantly correlated to cancer-associated fibroblast infiltration in TCGA HCC tumor samples. Moreover, inhibition of ERK1/2 suppressed tumor cell-induced enhancement of HSC migration and invasion by regulating expression of fibrosis markers FAP, FN1 and COL1A1. In a tumor cell and HSC splenic co-transplanted xenograft mouse model, inhibition of ERK1/2 suppressed liver tumor formation by downregulating fibrosis, indicating ERK1/2 inhibition suppresses tumor-stromal interactions *in vivo*. Taken together, our data indicate that inhibition of ERK1/2 in tumor-associated HSCs suppresses tumor-stromal interactions and progression. Furthermore, inhibition of ERK1/2 may be a potential target for HCC treatment.

Keywords: ERK1/2, extracellular matrix, hepatocellular carcinoma, hepatic stellate cell, tumor microenvironment

Introduction

Hepatocellular carcinoma (HCC) is the most common primary liver cancer and the second leading cause of cancer-related death worldwide [1]. The majority of patients with HCC are diagnosed at the advanced stage [2], and the lack of an effective treatment results in a poor overall prognosis, with a 5-year overall survival rate of 12% in China [3]. Despite the advancement of modern medicine and radical hepatectomy, the overall recurrence rate remains high and has not improved [4]. Therefore, the identification of novel therapeutic strategies and agents is required to improve the treatment and outcome of HCC patients [5].

Over 80% of HCC cases develop in the liver with fibrosis, and liver fibrosis is crucial in the occurrence, development and tumor microenvironment (TME) of liver cancer [6]. Activated hepatic stellate cells (HSCs) are the main component of HCC-related fibroblasts; these cells produce extracellular matrix (ECM) proteins and play a key role in liver fibrosis [7]. Through interactions with cancer cells and various stimuli, HSCs change from quiescent to activated fibroblasts. Activated fibroblasts secrete cytokines that promote the invasiveness and viability of cancer cells and produce ECM proteins and inflammatory cytokines to promote the progress of the TME, thus promoting the development of liver cancer [8]. α-Smooth muscle actin (α-SMA) is a

https://doi.org/10.62347/VPYE3817

marker protein for HSC activation in tumor lesions, and studies have shown that the survival period of liver cancer patients with high SMA expression is significantly shortened [9]. Recent reports have demonstrated that activated HSCs promote the tolerance of liver cancer to chemotherapy drugs such as sorafenib, regorafenib, 5-fluorouracil and cisplatin [10, 11]. Our previous studies found that pyroptosis of liver cancer cells inhibits the development of liver cancer by downregulating HSC activation and tumor-stromal interactions [12]. Therefore, targeting HSCs rather than cancer cells in the TME represents a potential HCC therapeutic strategy [13, 14].

Extracellular signal-regulated kinases (ERKs), also known as mitogen-activated protein kinases, are the integration points of various biochemical signaling pathways in humans and regulate transcription, differentiation, proliferation and development [15]. Phosphorylation of ERK1/2 plays an important role in autophagy, senescence and epithelial-mesenchymal transformation (EMT) in gastrointestinal tumors [16-18]. ERK1/2 inhibitors have thus been developed for the targeted treatment of cancer. In the TME of HCC, activated HSCs promote EMT and cell cycle of cancer cells through the ERK1/2 signal pathway [18]. Additionally, studies have shown that the inactivation of ERK1/2 effectively inhibited the development of HCC [19, 20]. Recent studies have found that the activation of HSCs is accompanied by autophagy activation and ERK1/2 phosphorylation [21]. In our previous research on the TME of pancreatic cancer, we found that the ERK1/2 inhibitor SCH772984 inhibits the fibrotic activation of stellate cells by promoting autophagy and cell senescence [22]. However, the functional role of ERK1/2 inactivation in the activation of HSCs and the mechanism of regulating tumor-stromal interactions has not been clarified to date.

In the present study, we investigated ERK1/2 inactivation in HCC fibrosis and tumor-stromal interaction in vitro and in vivo. Our high-throughput transcriptome sequencing (RNA-seq) analysis suggested that inactivation of ERK1/2 may significantly suppress adhesion abilities of HCCs and HSC by regulating ECM organization and focal adhesion. Inhibition of ERK1/2 suppressed the HCC-enhanced migration and invasion capacity of HSCs and this may be mediated by downregulation of FAP, FN1 and COL1A1, which are fibrosis markers. Furthermore, SCH-772984 effectively inhibited liver tumor formation in a xenograft mouse model. Our results indicated that ERK1/2 has potential as a target for the treatment of HCC tumor-stromal interaction.

Materials and methods

Patient samples

The liver tumor specimens were obtained from 8 patients who were diagnosed with HCC and underwent curative hepatectomies from 2012 to 2019 at Peking University Shenzhen Hospital (**Table 1**). The ethics committee of Peking University Shenzhen Hospital approved the use of specimens and follow-up information. All patients provided written informed consent.

Immunohistochemistry

Tissues were embedded and sliced into 4-μm-thick sections. Immunohistochemical staining and multiple fluorescent immunohistochemistry (abs50012, Absin, China) were used for multiplexed IHC (mIHC) as described in a previous study [12]. Sections were incubated with the following primary antibodies overnight at 4°C: anti-phospho-ERK1/2 (AP0472, ABclonal, China), anti-α-SMA (A17910, ABclonal), anti-FAPα (A6349, ABclonal), anti-COL1A1 (A16891, ABclonal) and anti-Fibronectin (A12932, ABclonal). Sections were then incubated with secondary antibodies using an SP-POD Kit (PV-6000, Zsbio, China). Images were acquired using a fluorescence microscope (DMi8, Leica, Germany). The statistical index utilized for immunohistochemistry analyses was defined as the percentage of tumor cells with positive expression compared to all tumor cells.

Cell lines and culture conditions

The human hepatic stellate LX-2 cell line and hepatocellular carcinoma cell lines MHCC97L, MHCC97H, Huh7, HepG2 and Hep3B (Chinese Academy of Medical Sciences, Beijing, China) were previously described [12]. All cell lines were maintained in Dulbecco's modified Eagle's medium (Gibco, Thermo Scientific, USA) supplemented with 10% fetal bovine serum (Gibco,

Table 1. The clinicopathological characteristics of patients used for IHC stain

Patient ID	Sex	Age	Diagnosis	Surgical procedure	Date of surgery	Other diagnosis	Pathological diagnosis
478794	M	52	Hepatocellular carcinoma	Open resection of liver lesions	2019/2/21	Portal vein tumor thrombus, post-hepatitic cirrhosis, chronic hepatitis B, acquired renal cyst, chronic cholecystitis, primary hypertension	Hepatocellular carcinoma
437793	F	35	Hepatocellular carcinoma	Open resection of liver lesions	2018/2/28	Chronic hepatitis B	Hepatocellular carcinoma
415545	M	44	Hepatocellular carcinoma	Open resection of liver lesions	2018/4/10	Chronic hepatitis B	Well differentiated hepatocellular carcinoma
325184	M	32	Hepatocellular carcinoma	Open resection of liver lesions	2018/9/20	Chronic hepatitis B	Hepatocellular carcinoma
9894	M	80	Hepatocellular carcinoma	Open resection of liver lesions	2014/9/25	Personal history of colon cancer and prostate cancer, hypertension	Hepatocellular carcinoma
18841	M	54	Hepatocellular carcinoma	Open resection of liver lesions	2014/1/7	Chronic hepatitis B, personal history of liver cancer	Well differentiated hepatocellular carcinoma
28516	M	55	Hepatocellular carcinoma	Open resection of liver lesions	2014/7/24	Chronic hepatitis B	Moderately differentiated hepatocellular carcinoma in right lobe of liver
32118	M	67	Hepatocellular carcinoma	Open resection of liver lesions	2012/10/24	Decompensated stage of liver cirrhosis, hypoalbuminemia, malignant hypertension, Chronic hepatitis C, hepatic cyst, moderate anemia	Medium to low differentiated hepatocellular carcinoma

Thermo Scientific), 100 U/ml penicillin and 100 U/ml streptomycin (Life Technologies) in a humidified atmosphere with 5% CO_2 at 37°C.

qRT-PCR

Total RNA was extracted using the RNAeasy™ Animal RNA Isolation Kit (R0026, Beyotime, China) following the manufacturer's instructions. qRT-PCR was performed with the iTaq™ Universal SYBR Green One-Step Kit (1725150, Bio-Rad Laboratories, USA) and monitored using an ABI PRISM 7500 Sequence Detection System (Applied Biosystem, Life Technologies). The primer sequences were as follows: TGF-β1: Forward, 5'-GGCCAGATCCTGTCCAAGC-3'; Reverse, 5'-GTGGGTTTCCACCATTAGCAC-3'; acta2: Forward, 5'-AAAAGACAGCTACGTGGGTGA-3'; Reverse, 5'-GCCATGTTCTATCGGGTACTTC-3'; FAP: Forward, 5'-ATGAGCTTCCTCGTCCAATTCA-3'; Reverse, 5'-AGACCACCAGAGAGCATATTTTG-3'; FN1: Forward, 5'-CGGTGGCTGTCAGTCAA-AG-3'; Reverse, 5'-AAACCTCGGCTTCCTCCATAA-3'; and COL1A1: Forward, 5'-GAGGGCCAAGA-CGAAGACATC-3'; Reverse, 5'-CAGATCACGTCA-TCGCACAAC-3'.

Western blot analysis

Cells were lysed using RIPA Lysis Buffer (G2002-100 ml; Servicebio Biotechnology, Wuhan, China) and protein concentrations were determined using the BCA Protein Assay Kit (P0012S; Beyotime). The proteins were resolved on SDS-PAGE gels and transferred to a PVDF membrane. The membranes were incubated with primary antibodies at 4°C overnight, followed by incubation with secondary antibodies at room temperature for 2 h. Membranes were washed in TBS-Tween 0.1% between steps. The primary antibodies used in this study were as follows: anti-phospho-ERK1/2 (AP0472, ABclonal), anti-α-SMA (A17910, ABclonal), anti-FAPα (A6349, ABclonal), anti-COL1A1 (A16891, ABclonal), anti-Fibronectin (A12932, ABclonal) and anti-b-actin (3700T, Cell Signaling Technology, USA). The immunoreactive bands were detected using the appropriate HRP-conjugated secondary antibodies from Abcam.

Invasion and migration assays

Transwell chambers with and without Matrigel (20 μg/well, BD Biosciences, USA) coating were used to perform migration and invasion assays as previously described [23]. A total of 5×10^4 cells/250 μL of medium were added to the upper chambers (8-μm pore size, Costar, USA) and 750 μl of medium was added to the bottom chamber. After incubation of 24 h (for migration assays) or 48 h (for invasion assays), the cells on the lower surface of the membrane were fixed in 4% paraformaldehyde and stained with hematoxylin-eosin. The number of invaded or migrated cells was quantified in five random fields using a light microscope (DMi8, Leica).

Cell viability assay

Cells (2×10^3 cells/well) were added in BeyoGold™ 96-Well White Opaque Plates (FCP968, Beyotime). Cell viability was determined using the CellTiter-Lumi™ II Luminescent Cell Viability Assay Kit (C0056S, Beyotime).

Adhesion assay

Control or ERK1/2 inhibitor-treated cells (IC50 dose concentration, 2×10^5/well) were dyed with CMFDA CellTracker (40721ES50, Yeasen, China) and seeded into 24-well plates coated with collagen I (WHB-24-CC, WHB-bio, China). After 3 h, plates were washed three times with 500 μL phosphate-buffered saline (PBS) to remove non-adherent cells. The numbers of adhered cells were counted in five random fields using a fluorescent microscope (DMi8, Leica) at × 100 magnification.

Co-culture migration assay

The migration ability of cells in co-culture was determined using wound healing assays as previously described [12]. Cancer cells were labeled with Cell Tracker Green and LX-2 cells were labeled with Cell Tracker Red; the cell lines were seeded into each side of a co-culture insert (81176, ibidi, Germany). At 24 h after cells were seeded, the insert was removed and the cells began to migrate. The width of the wound was monitored and measured at various times. LX-2 activation was performed by treating cells with 10 ng/mL recombinant TGF-β1 (Solarbio, P00121, China) for 24 h; For collection of supernatant, the cancer cells cultured for 7 days were washed twice with PBS and the fresh medium was replaced. After 48 h incubation at 37°C, the medium was collected and filtered with a 0.22-μm syringe filter (Z359904; Merck, Germany). After centrifuga-

tion at 1,500 rpm for 5 min, the supernatants were collected.

High-throughput transcriptome sequencing

Cultured cells were collected and stored in TRIzol reagent. The total RNA extraction, RNA quality evaluation and the related analyses were carried out by Novogene Co., Ltd. (China). The sequencing data have been deposited in the NCBI Sequence Read Archive (SRA) database under the accession code PRJNA921975.

In vivo experiments

Four-week-old BALB/c athymic female nude mice were obtained from Model Organisms (Shanghai, China). After 7 days of acclimatization, mice were splenic co-transplanted with 5 × 10^5 MHCC97H cells and 5 × 10^5 LX-2 cells and randomized into PBS or SCH772984 treatment groups (n = 5/group). At 14 days after transplantation, mice were intraperitoneal drug dosed once daily with vehicle or SCH772984 (25 mg/kg) for 14 days. The mice were sacrificed and liver lesions were collected for subsequent analyses. All mouse experiments were approved by the Peking University Shenzhen Hospital Animal Care Committee (Shenzhen, China, No. 2023-140, June 21, 2023).

Database-based bioinformatics data mining

Human Protein Atlas [24] (http://www.proteinatlas.org) and The Cancer Genome Atlas (TCGA, http://www.cancer.gov/tcga) datasets were used to investigate the expression of hepatocellular carcinoma in this study. UALCAN [25] (http://ualcan.path.uab.edu/index.html), GEPIA2 [26] (http://gepia2.cancer-pku.cn/#index), GSCA: Gene Set Cancer Analysis [27] (http://bioinfo.life.hust.edu.cn/GSCA/) and SRplot (http://www.bioinformatics.com.cn/srplot) were used for tumor gene expression, survival analyses and bioinformatics analyses.

Statistical analysis

Comparisons of RNA expression in bioinformatic analyses were determined using the Kruskal-Wallis test and Wilcox test. Statistical analyses were performed using GraphPad Prism 8 and R language. $P < 0.05$ indicated statistical significance.

Results

ERK1/2 overexpression is correlated with the poor prognosis of HCC patients

On examination of the Human Protein Atlas database [24], we observed varying expressions of ERK1 and ERK2 in HCC, including negative, weak, medium, and strong expression (**Figure 1A**, **1B**). Analysis using UALCAN [25] showed that the expressions of ERK1 and ERK2 were markedly upregulated in HCC tumor tissues compared with normal liver tissues (**Figure 1C**). Further analysis using GEPIA2 [26] showed that the high expressions of ERK1 and ERK2 correlated with poor overall survival in HCC (**Figure 1D**). Furthermore, the expressions of ERK1 and ERK2 in HCC were correlated with histological subtypes, TP53 mutation and nodal metastasis (Figures S1 and S2). From the bioinformatics analysis of TCGA and Genotype-Tissue Expression Project (GTEx) database [28], we found that the expressions of ERK1 and ERK2 were highly correlated in normal liver tissues and HCC tumor tissues (**Figure 1E**).

ERK1/2 activation is involved in fibrosis of HCC tumors

Different from normal liver tissues, HCC tissues exhibited extension fibrosis and high-level ERK1/2 phosphorylation [29]. α-SMA is a biomarker of HSC activation and liver fibrosis. The expression of α-SMA was associated with tumor recurrence and overall survival in patients with HCC [9]. We performed Masson's trichrome staining of HCC specimens from our institution and found a strong elevation of collagen fibers in HCC. The increased collagen fiber and overexpression of α-SMA indicates fibrosis in the TME of HCC (**Figure 2A**). We subsequently found co-localization between phosphorylated ERK1/2 and α-SMA using multiple fluorescent immunohistochemical staining (**Figure 2B**). We also investigated the protein expressions of α-SMA and phosphorylation of ERK1/2 in normal liver cells and HCC cells. As shown in **Figure 2C**, human HSC LX-2 cell, HCC cell line MHCC97H and Huh7 cell exhibited high levels of ERK1/2 phosphorylation compared to normal L02 cells. These results suggested that ERK1/2 phosphorylation may be involved in HSC activation and HCC tumor fibrosis.

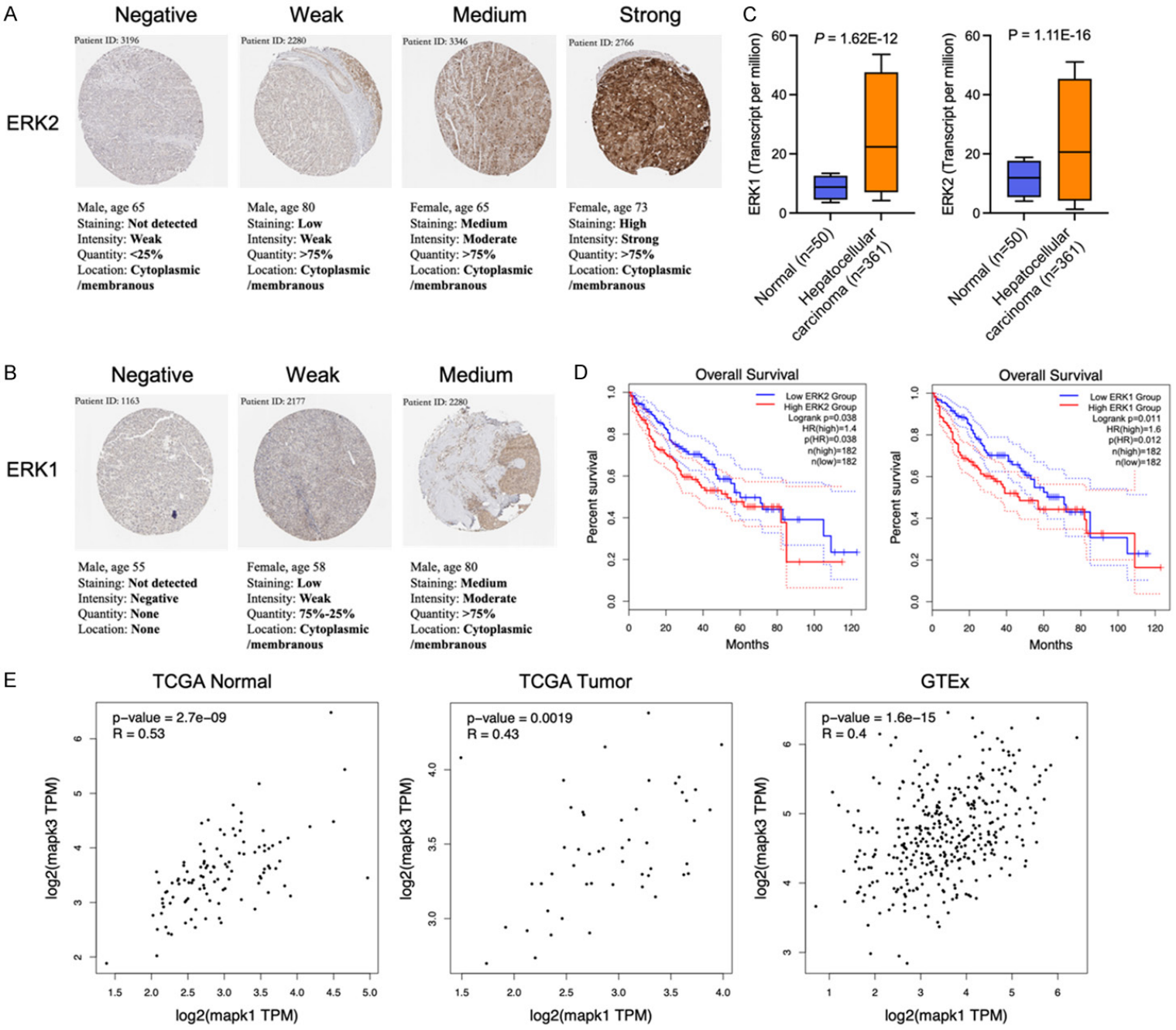
A
Negative
Weak
Medium
Strong
ERK2
Patient ID: 3196
Patient ID: 2280
Patient ID: 3346
Patient ID: 2766
Male, age 65
Staining: Not detected
Intensity: Weak
Quantity: <25%
Location: Cytoplasmic /membranous
Male, age 80
Staining: Low
Intensity: Weak
Quantity: >75%
Location: Cytoplasmic /membranous
Female, age 65
Staining: Medium
Intensity: Moderate
Quantity: >75%
Location: Cytoplasmic /membranous
Female, age 73
Staining: High
Intensity: Strong
Quantity: >75%
Location: Cytoplasmic /membranous
C
P = 1.62E-12
P = 1.11E-16
ERK1 (Transcript per million)
ERK2 (Transcript per million)
Normal (n=50)
Hepatocellular carcinoma (n=361)
B
Negative
Weak
Medium
ERK1
Patient ID: 1163
Patient ID: 2177
Patient ID: 2280
Male, age 55
Staining: Not detected
Intensity: Negative
Quantity: None
Location: None
Female, age 58
Staining: Low
Intensity: Weak
Quantity: 75%-25%
Location: Cytoplasmic /membranous
Male, age 80
Staining: Medium
Intensity: Moderate
Quantity: >75%
Location: Cytoplasmic /membranous
D
Overall Survival
Low ERK2 Group
High ERK2 Group
Logrank p=0.038
HR(high)=1.4
p(HR)=0.038
n(high)=182
n(low)=182
Percent survival
Months
Overall Survival
Low ERK1 Group
High ERK1 Group
Logrank p=0.011
HR(high)=1.6
p(HR)=0.012
n(high)=182
n(low)=182
Percent survival
Months
E
TCGA Normal
p−value = 2.7e−09
R = 0.53
log2(mapk3 TPM)
log2(mapk1 TPM)
TCGA Tumor
p−value = 0.0019
R = 0.43
log2(mapk3 TPM)
log2(mapk1 TPM)
GTEx
p−value = 1.6e−15
R = 0.4
log2(mapk3 TPM)
log2(mapk1 TPM)

Figure 1. Bioinformatics analysis of the expression of ERK2 and ERK1 in liver cancer. A, B. Expressions of ERK2 and ERK1 in HCC tissues. C. The expressions of ERK2 (P = 1.62E-12) and ERK1 (P = 1.11E-16) were significantly upregulated in HCC tumor tissues compared with tumor-adjacent normal tissues. D. Kaplan-Meier survival analysis of overall survival of HCC patients in accordance with ERK2 and ERK1 expression. Overexpression of ERK2 and ERK1 was associated with shorter patient survival times (log-rank P = 0.038 and 0.011). E. Correlations between ERK2 and ERK1 in TCGA normal, TCGA tumor and GTEx databases.

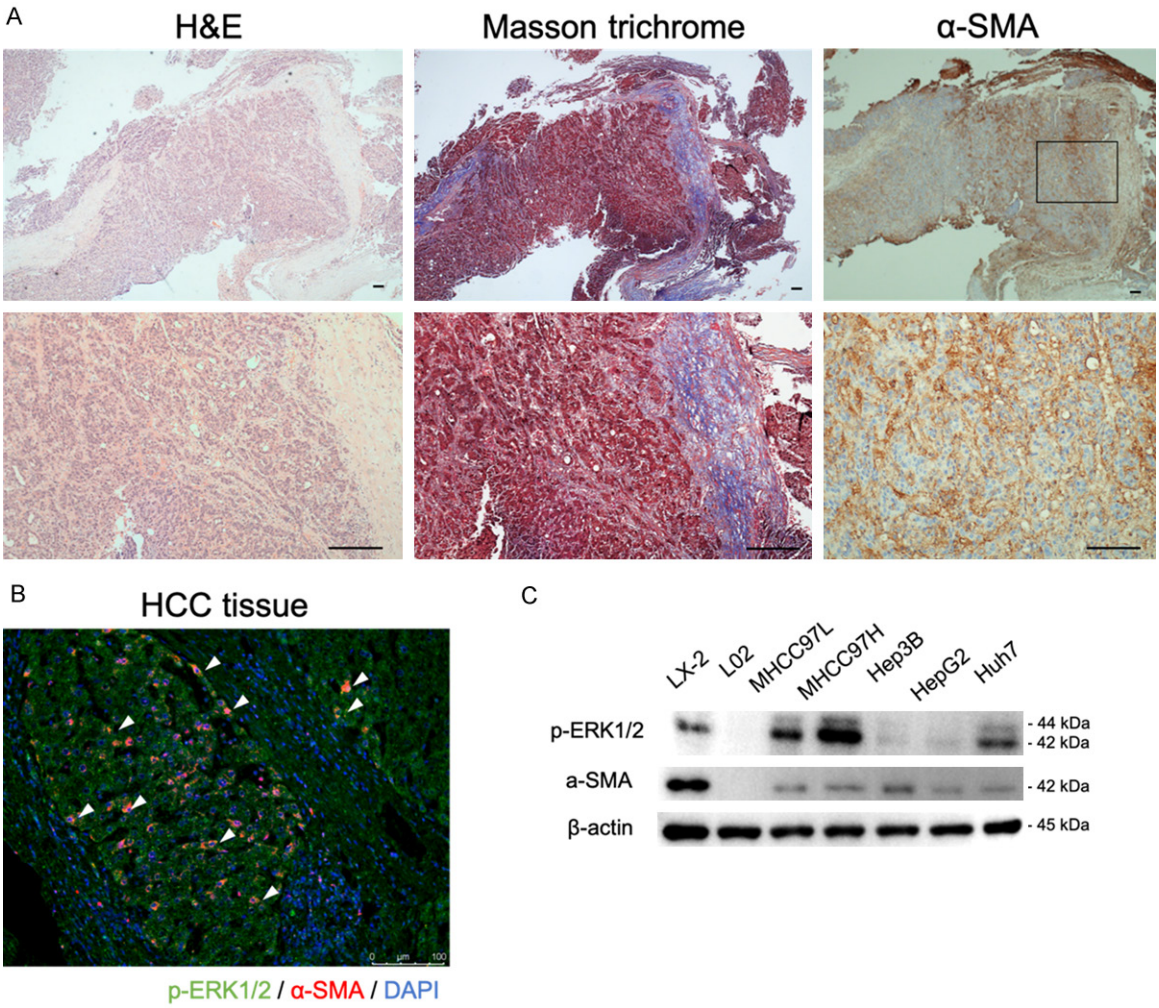

Figure 2. Activation of ERK1/2 is involved in fibrosis of HCC. A. Masson trichrome and immunohistochemical staining of α-SMA in HCC specimens. B. Co-localization of ERK1/2 and α-SMA was observed on serial sections of HCC specimens. Scale bars = 100 μm. C. Protein levels of p-ERK1/2 and α-SMA in LX-2, L02 and HCC cells.

HCCs stimulate activation of LX-2 cells by ERK1/2 phosphorylation

The tumor-stromal interaction plays a crucial role in HCC development [30]. In HCC tumors, the activation of HSCs leads to strengthened tumor-stromal interactions [31, 32]. Using a transwell co-culture model, we observed that the addition of TGFβ-1 recombinant protein or cancer cell supernatants significantly stimulated activation of the human HSC cell line LX-2, as observed by increased α-SMA expression; notably these factors also induced p-ERK1/2 levels upregulation (**Figure 3A**). We also found that the invasiveness and migratory abilities of LX-2 cells were enhanced when cells were co-cultured with TGFβ-1 recombinant protein or cancer cell supernatant (**Figure 3B**).

The ERK inhibitor SCH772894 suppresses HCC cell-mediated effects of HSCs

To investigate the role of ERK1/2 in HSCs and HCC, we used SCH772984, a highly selective

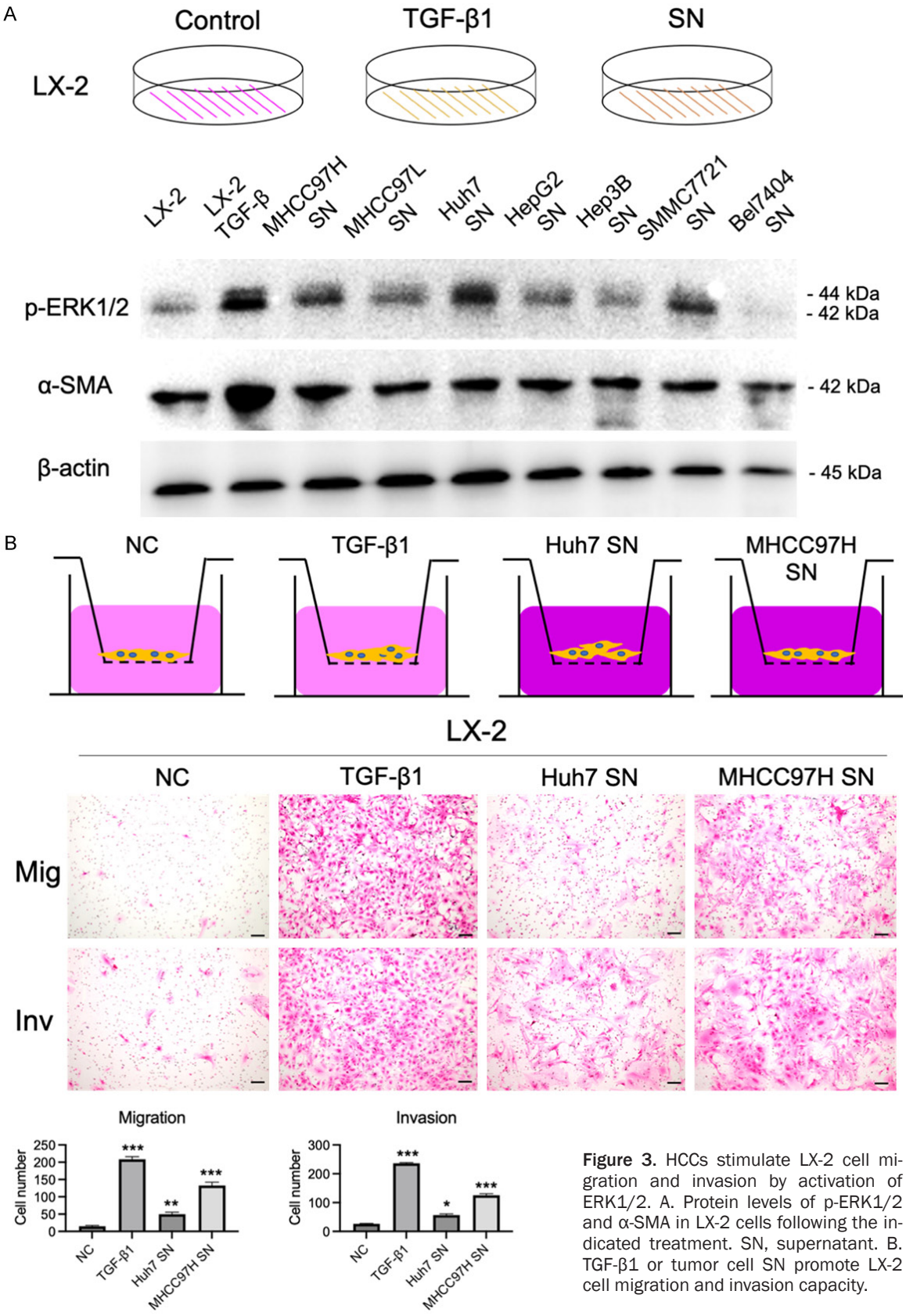

Figure 3. HCCs stimulate LX-2 cell migration and invasion by activation of ERK1/2. A. Protein levels of p-ERK1/2 and α-SMA in LX-2 cells following the indicated treatment. SN, supernatant. B. TGF-β1 or tumor cell SN promote LX-2 cell migration and invasion capacity.

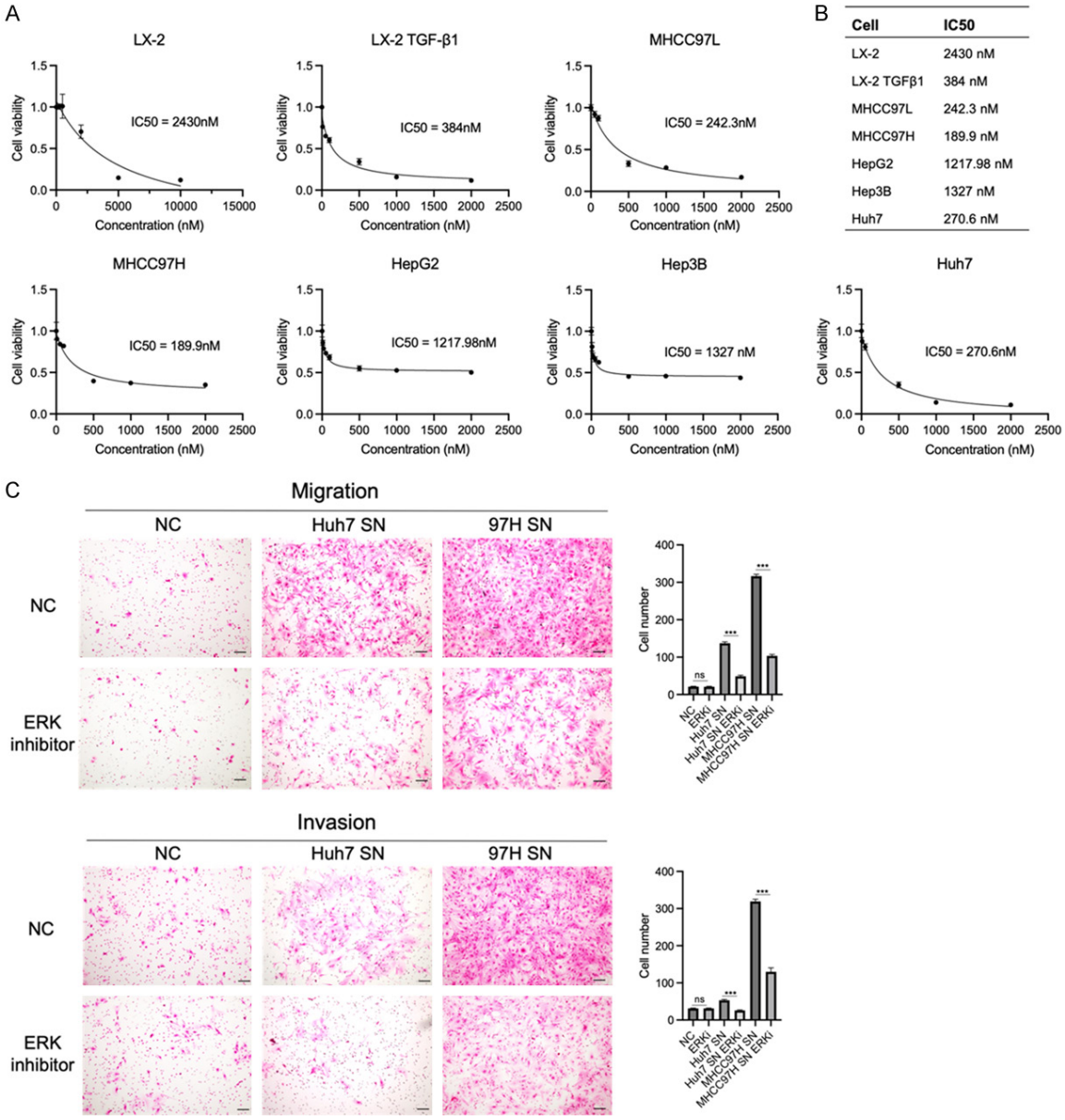

Figure 4. SCH772984 suppresses tumor-stromal interactions in HSCs that enhance migration and invasiveness. A. Viability of LX-2, TGF-β1-treated LX-2, MHCC97L, MHCC97H, HepG2, Hep3B and Huh7 cells after 48 h treatment with various concentrations of the ERK inhibitor SCH772984. B. IC50 values are indicated. C. Migration and invasion assays were performed for 24 and 48 h with tumor cell supernatant and/or ERK inhibitor. Graphs show the numbers of cells calculated from five fields. Scale bars = 100 μm. ***P < 0.001.

ERK1/2 inhibitor that was shown to suppress tumor growth in mouse models without toxicity [33]. We examined the drug sensitivity of HSCs and HCC cells to SCH772984 and calculated the IC50 value (**Figure 4A**). LX-2 cells activated by TGFβ-1 recombinant protein treatment showed a significantly increased sensitivity to SCH772984 (**Figure 4B**), indicating the potential of ERK1/2 suppression in HSC inactivation. Furthermore, SCH772984 did not decrease the migratory or invasiveness of LX-2 cells treated with the lower IC50 dose for TGFβ1-treated LX-2 cells using a transwell coculture system. However, the lower dose of SCH772984 decreased the migratory or invasiveness of LX-2 cells in the presence of MHCC97H or Huh7 cell supernatant (**Figure 4C**).

ERK1/2 inactivation suppresses ECM remodeling and adherent ability of HCC cells and HSCs

To further explore the underlying mechanisms of ERK1/2 in HCC and HSC, we conducted high-throughput RNA sequencing in cells after ERK1/2 inhibition. A total of 1881 differentially expressed genes were observed in ERK1/2-inhibited LX-2 cells compared with control LX-2 cells and 975 differentially expressed genes were found in ERK1/2-inhibited MHCC97H cells compared with control MHCC97H cells (**Figure 5A**, **5B**). Gene Ontology (GO) and Kyoto Encyclopedia of Genes and Genomes (KEGG) terms showed that a proportion of differentially expressed genes was significantly associated with signaling pathways involved in ECM, collagen, migration and adhesion in LX-2 cells and ECM, TGFβ, motility and migration in MHCC97H cells (**Figures 5C**, **5D** and S3A, S3B). Notably, we identified a remarkable correlation between the differentially expressed genes and ECM remodeling: "extracellular structure organization" and "extracellular matrix organization" were in the top 10 GO Biological Process (BP) pathways, whereas "extracellular matrix" and "proteinaceous extracellular matrix" of GO Cellular Component (CC) pathways, "extracellular matrix structural constitute" and "extracellular matrix binding" of GO Molecular Function (MF) pathways were significantly correlated; these results suggest mechanisms that might contribute to the tumor-stromal interaction and cell adhesion in hepatocellular carcinoma progression (**Figures 5C**, **5D** and S3A, S3B). ECM-receptor interaction and focal adhesion in KEGG pathways were observed in both ERK1/2-inhibited aLX-2 and MHCC97H cells (**Figure 5E**, **5F**).

We next performed adhesion assays of HCC cells and HSCs to collagen I and found that the adherent capacity of cells was significantly downregulated following ERK1/2 inhibition (**Figure 5G**). Given the importance of ERK1/2 inhibition in ECM remodeling and adhesion ability of HCC and HSCs, we suggest that ERK1/2 inhibition may be a potential strategy for HCC treatment.

ERK1/2 inhibition-related gene set correlated to CAF infiltration

We next investigated the mechanism of ERK1/2 inhibition in the HCC TME. As the most important component in the TME, cancer-associated fibroblasts (CAFs) originate from activated HSCs and play a critical role in HCC fibrosis [7, 8]. Through analyzing the overlapping differentially expressed genes in LX-2 and MHCC97H cells after ERK1/2 inhibition, we screened a gene set including 22 prognostic genes of the intersecting genes (**Table 2**). We next analyzed the gene set using Gene Set Cancer Analysis (GSCA, http://bioinfo.life.hust.edu.cn/GSCA/#/) [27] to generate a gene set variation analysis score (**Figure 6A** and Table S1). We assessed the CAF infiltration level in TCGA HCC tumor samples using R package of EPIC, xCell, MCPcounter and Estimate (**Figure 6B** and Table S2). We found that the gene set variation analysis score was significantly highly correlated to CAF infiltration levels determined by EPIC, xCell, MCPcounter and Estimate, which suggests a strong correlation between the ERK1/2 inhibition-related gene set and CAF infiltration in HCC (**Figure 6C**).

ERK1/2 inactivation suppresses HCC tumor-stromal interactions in vitro

HCC cells and HSCs exhibited similar reactions to ERK1/2 inhibition; therefore, we examined the effect of ERK1/2 inhibition on the tumor-stromal interaction. We performed a wound-healing assay to examine tumor-stromal interactions using LX-2 cells and cancer cells. We found that SCH772984 inhibited the tumor-stromal interaction by suppressing cell migration toward cells (**Figure 7A**). Next, we investigated changes in expressions of related markers that may be involved in fibrosis after SCH772984 treatment. We found that TGFβ-1, α-SMA, fibronectin 1 (FN1), fibroblast activation protein-α (FAP) and collagen type I alpha 1 (COL1A1), which are involved in tumor-stromal interaction and tumor progression, were downregulated after SCH772984 treatment (**Figure 7B**, **7C**).

ERK1/2 inactivation suppresses tumor-stromal interactions and HCC progression in vitro

MHCC97H cells and aLX-2 cells were co-transplanted into spleens of nude mice. Two weeks later, mice were intraperitoneally administrated PBS or SCH77298 once daily for 14 days (**Figure 8A**). At the end of the treatment period, the liver lesions were harvested (**Figure 8B**). Compared with the control treatment, SCH-772984 treatment remarkably decreased liver

Inactivation of ERK1/2 suppressed cancerstromal interaction

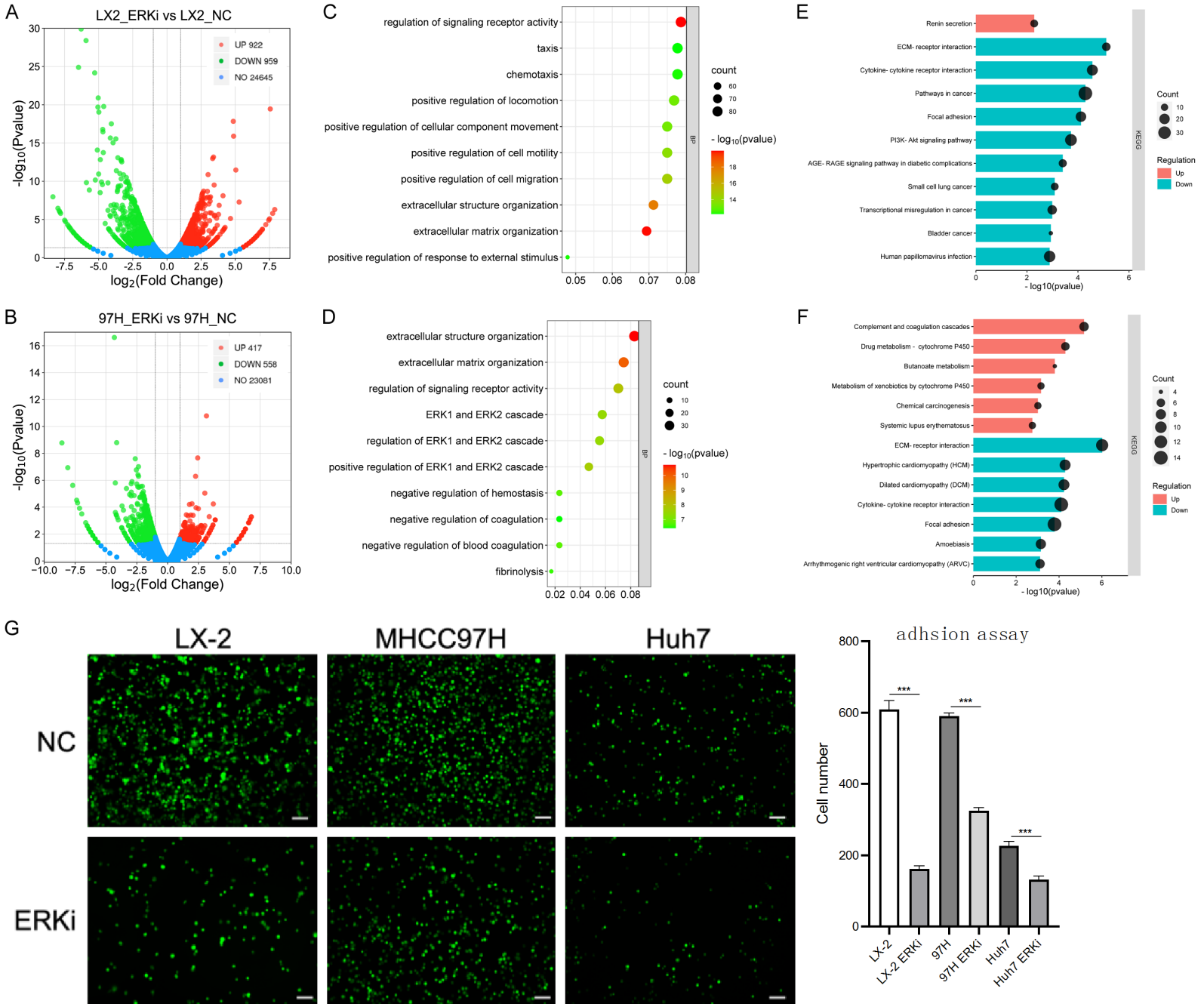

Figure 5. ERK1/2 inhibition correlated with ECM remodeling and cell adhesion in HCCs. A, B. Volcano plots of RNA expression profiles showing differentially expressed genes in aLX-2 and MHCC97H cells with ERK1/2 inhibition. C, D. Gene Ontology enrichment analysis of top 10 biological process terms in aLX-2 cells and MHCC97H cells. The size of the dots represents the number of genes; a larger dot indicates a larger number of genes in the corresponding process. E, F. Kyoto Encyclopedia of Genes and Genomes pathways in aLX-2 cells and MHCC97H cells. The size of the dots represents the number of genes. The red bars represent upregulated pathways and blue bars represent downregulated pathways. G. Cells were dyed with Cell Tracker green and examined for adhesion ability to collagen. Graphs show the quantification of cells calculated from five fields. Original magnification, × 100; ***P < 0.001.

Table 2. Correlations between ERK1/2 inhibition-related genes and survival significance of TCGA HCC patients

Gene symbol	Higher risk of death	Overall survival *p*-value	LX-2 ERKi log2FoldChange	*P*-value	MHCC97H ERKi log2FoldChange	*P*-value
PTHLH	Higher expression	0.047	-1.941291723	1.41E-05	-2.112485994	0.000150551
PRSS35	Higher expression	0.0016	5.593083467	0.040964585	1.871946643	0.000385548
VCAN	Higher expression	0.023	-1.431365372	0.000776806	-1.534962192	0.000642489
ARL14	Higher expression	0.033	1.872742057	0.014380224	-1.767946616	0.001161167
SUGT1P1	Higher expression	0.018	1.717823979	0.006493106	3.674640407	0.002133716
PDE2A	Lower expression	0.011	-1.543784869	0.00032523	-2.022940011	0.003217043
DNER	Higher expression	0.02	-1.908217756	1.19E-05	-1.938353752	0.00512978
P2RY2	Higher expression	0.022	-2.555416339	0.02704271	-1.228871492	0.005377006
NES	Higher expression	0.035	-1.282038832	0.0082961	-1.133736863	0.006457716
MMP1	Higher expression	0.0012	-5.924830878	4.02E-29	-1.218119967	0.007020677
STX1A	Higher expression	<0.0001	-1.504980004	0.000493534	-1.117800438	0.008090964
TGFB1	Higher expression	0.042	-1.180259464	0.004615661	-1.101259157	0.00822189
SOCS2	Lower expression	0.0077	1.115492865	0.026176488	-1.298361468	0.011468932
GPR3	Higher expression	0.011	-2.295065263	4.94E-06	-1.243002446	0.01226986
SERPINE1	Higher expression	0.02	-1.464442078	0.0004682	-1.02753642	0.013251239
CYP24A1	Higher expression	0.013	-4.317609041	6.40E-07	-1.00866971	0.015071537
CFB	Lower expression	0.019	2.197608771	4.50E-06	1.895554111	0.018003167
HPDL	Higher expression	0.03	-1.615823352	0.026720022	3.095788335	0.021566548
GDAP1L1	Higher expression	0.041	-6.361998874	0.004174171	3.095788335	0.021566548
LRP11	Higher expression	0.0062	1.153209446	0.01086116	1.078640391	0.024852735
CCL26	Higher expression	0.022	1.245918399	0.018950166	-1.03981667	0.025986633
VCAM1	Higher expression	0.027	3.683222684	5.75E-05	-1.008830303	0.030944281

weight (average: 3.43 g vs. 1.85 g) and the liver volume (average: 2.625 vs. 1.88 cm^3) (**Figure 8C**, **8D**). Immunohistochemical staining of serial sections showed that the expressions of α-SMA (13% positive vs. 33% positive), COL1A1 (8% positive vs. 36% positive), FN1 (24% positive vs. 53% positive) and FAP (15% positive vs. 77% positive) were downregulated in the treatment group compared with the control group (**Figure 8E**). The corresponding dash lines indicated tumor area of the liver lesions. In addition, Masson's trichrome stain revealed a reduction in the expression of collagen fibers (22% positive vs. 33% positive) in the ERK1/2 inhibition group compared with the control group (**Figure 8E**). Taken together, these results indicated that inactivation of ERK1/2 suppressed HCC tumor-stromal interactions and tumor formation *in vivo*.

Discussion

In our study, we examined ERK1/2 in HCC and HSCs and its functional involvement in the HCC tumor-stromal interaction. Our data demonstrated that ERK1/2 activation is stimulated accompanied by HCC fibrosis and HCC-HSC interactions. Inactivation of ERK1/2 in HCC and HSCs induced suppression of adherent capacity and ECM-related signaling pathway alterations. In a mouse model, the ERK1/2 inhibitor SCH772984 suppressed tumor-stromal interactions via downregulation of tumor fibrosis (**Figure 9**).

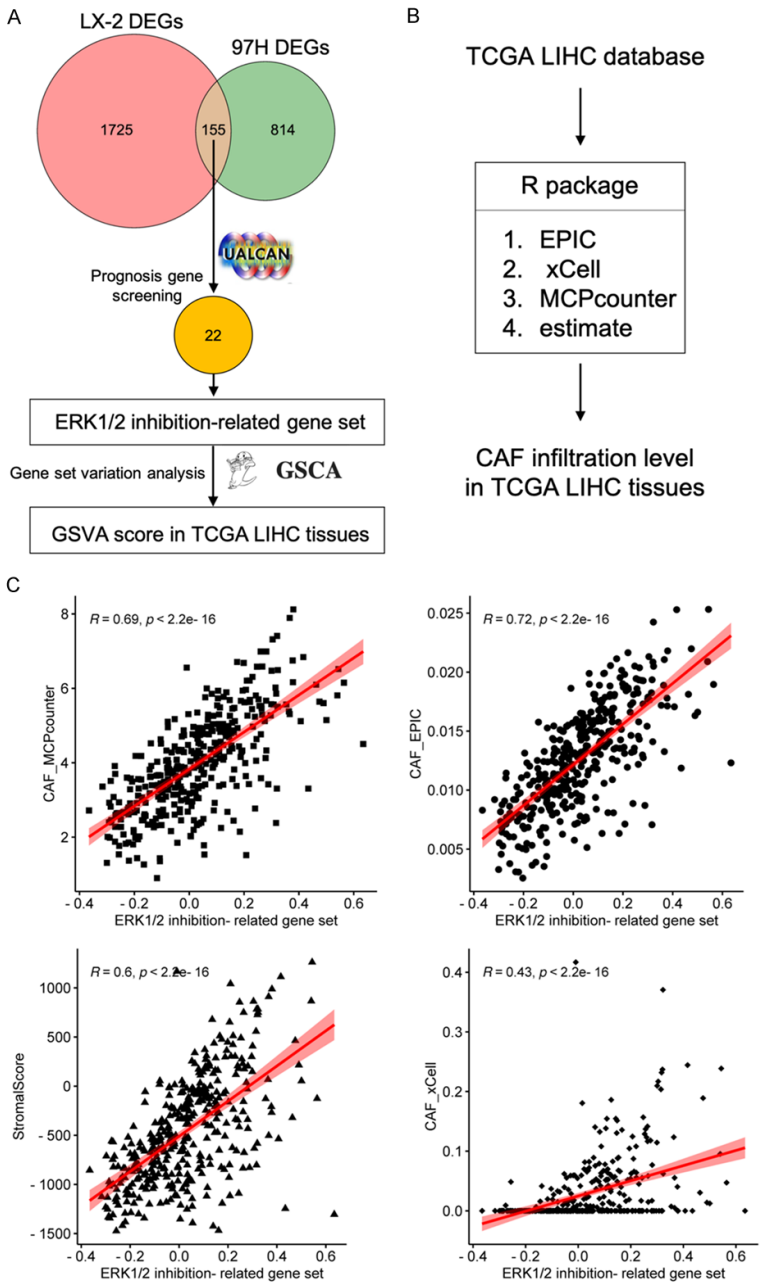

Figure 6. The ERK1/2 inhibition-related gene set significantly correlated with CAF infiltration in HCC. A. Scheme of the ERK1/2 inhibition-related gene set screening process. B. The R package of EPIC, xCell, MCPcounter, and Estimate were used for the evaluation of CAF infiltration score. C. Correlation between the ERK1/2 inhibition-related gene set and EPIC, xCell, MCPcounter, and Estimate.

Previous studies that indicated the involvement of ERK1/2 activation in EMT, cell proliferation and metastasis were focused mainly on cancer cells [18]. The expression of p-ERK1/2 has prognostic implication in HCC. However, α-SMA, a marker protein of HSC, also correlated with the prognosis of HCC. Our result showed co-localization of α-SMA and p-ERK1/2, demonstrating evidence of ERK1/2 activation in HSCs. Our result showed that activated HSCs stimulated by TGF-β1 or tumor cell supernatant had high levels of ERK1/2 phosphorylation, and activated HSCs were more sensitive to the ERK1/2 inhibitor. Furthermore, ERK1/2 activation also increased in HSCs following addition with tumor cell conditioned medium. These findings indicate that HCC may promote HSC activation and tumor-stromal interactions by regulating the phosphorylation of ERK1/2. Our study focused on the inactivation of ERK1/2 in HSCs but not traditional tumor cells. Recent studies reported that everolimus, curcumin, erlotinib and all-trans retinoic acid inhibit HCC progression via suppression of HSC activation [34-37]. Furthermore, the HSC-targeting drugs H3B-6527 and Fisogatinib are currently in Phase I clinical trials for treatment of HCC (https://clinicaltrials.gov/ct2/show/NCT-02834780; https://clinicaltrials.gov/ct2/show/NCT0250-8467). These findings suggest that targeting HSCs may be a new therapeutic approach for HCC.

Extensive deposition of ECM components is a typical feature of fibrosis [38]. In fibrotic livers, ECM is formed by accumulation of collagen type I and III, as well as non-collagenous glycoproteins like fibronectin, hyaluronan and laminin [39]. ECM plays a critical role in tumor cell invasion and metastasis. ECM is modified to enhance the attachment of cancer cells through alterations in cell-ECM adhesion dynamics to establish a growth factor-rich niche for invasion or metastasis [40]. CAFs serve as the principal cell type of ECM production and remodeling in

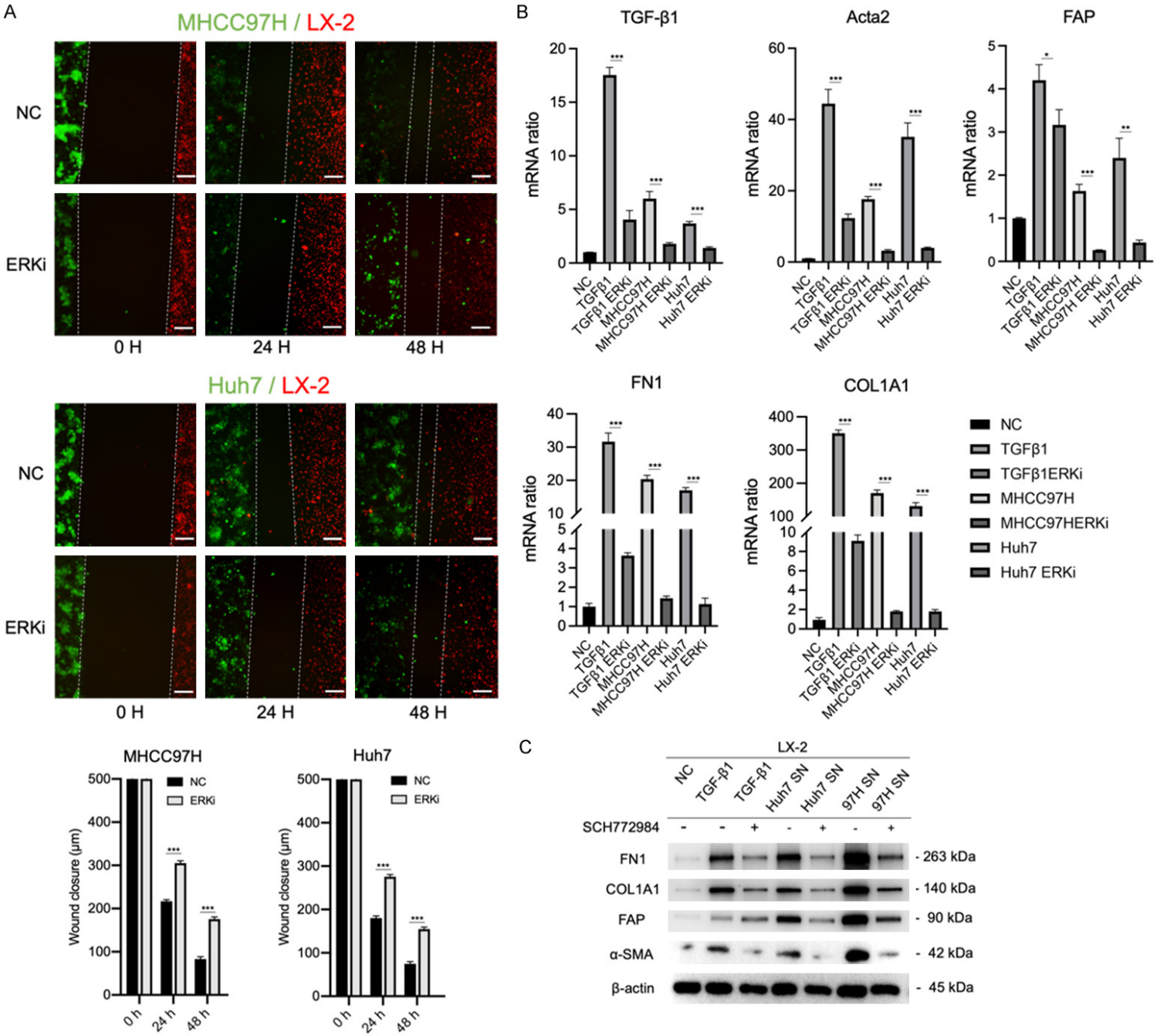
A
MHCC97H / LX-2
NC
ERKi
0 H
24 H
48 H
Huh7 / LX-2
NC
ERKi
0 H
24 H
48 H
MHCC97H
Huh7
Wound closure (μm)
NC
ERKi
0 h
24 h
48 h
B
TGF-β1
Acta2
FAP
FN1
COL1A1
mRNA ratio
NC
TGFβ1
TGFβ1 ERKi
MHCC97H
MHCC97H ERKi
Huh7
Huh7 ERKi
C
LX-2
NC
TGF-β1
TGF-β1
Huh7 SN
Huh7 SN
97H SN
97H SN
SCH772984
FN1
COL1A1
FAP
α-SMA
β-actin
263 kDa
140 kDa
90 kDa
42 kDa
45 kDa

Figure 7. SCH772984 suppresses tumor-stromal interactions by regulation of HSC fibrosis. A. MHCC97H or Huh7 cells were dyed with CellTracker Green, LX-2 cells were dyed with CellTracker Red, and migration assay was performed for 12 and 24 h. Original magnification: × 100. Scale bars = 100 μm. ***P < 0.001. B. qRT-PCR of HSCs after ERK1/2 inhibition. *P < 0.05, **P < 0.01, ***P < 0.001. C. The protein levels of FN1, COL1A1, FAP and α-SMA in LX-2 cells following the indicated treatment.

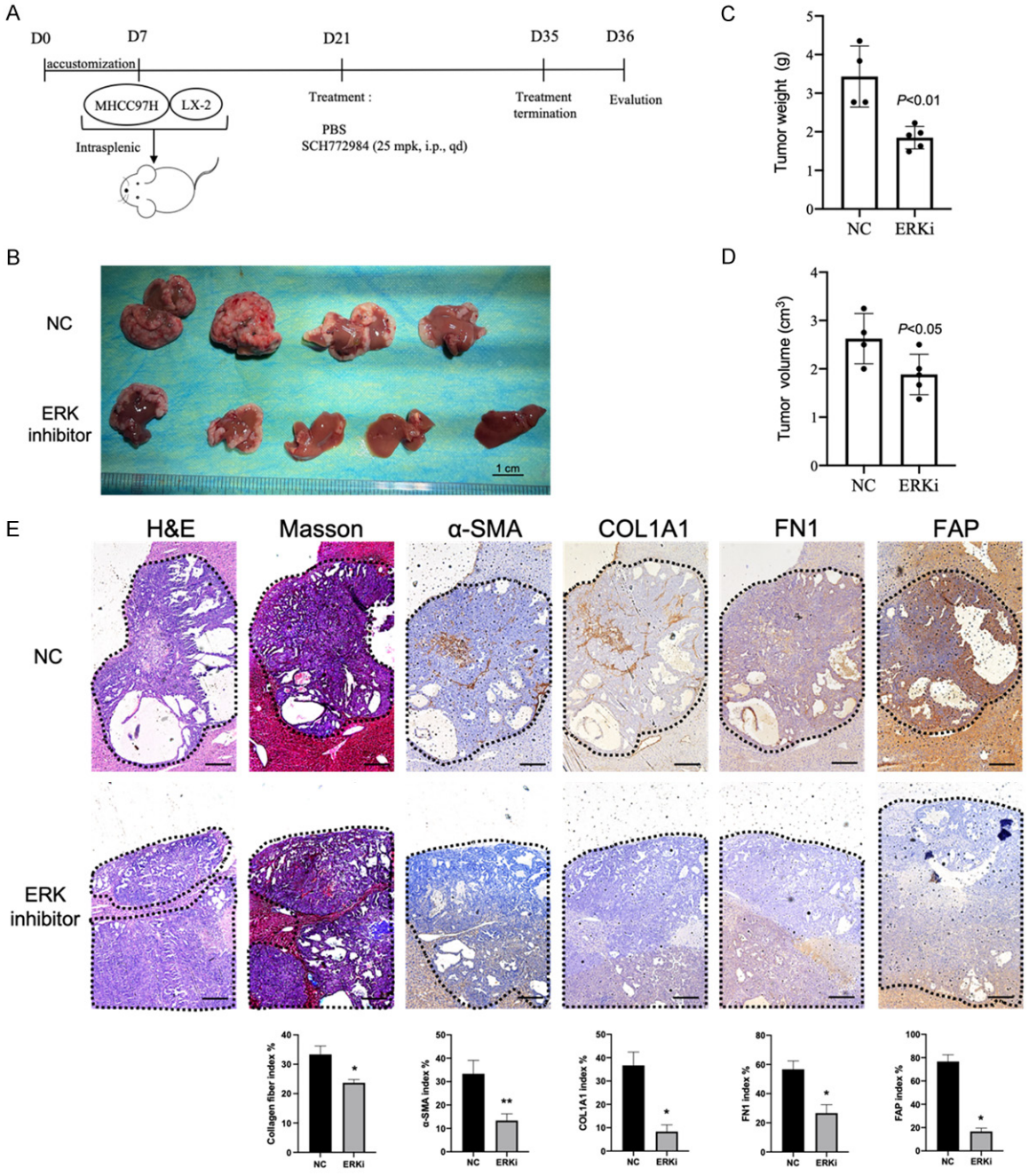

Figure 8. SCH772984 decreased HCC tumor formation in a xenograft model with HCC cell and HSC co-transplantation. A. Scheme of xenograft experiments. Female nude mice were intrasplenically transplanted with cancer cells with HSCs and randomized into two groups (n = 5/group). Two weeks after implantation, mice were dosed once daily with vehicle or SCH772984 (25 mg/kg) for two weeks; dosing occurred from day 21 to day 35. At day 36, mice were sacrificed and liver tumor lesions were harvested. B. Gross pathology showed that inhibition of ERK1/2 significantly suppressed tumor formation of liver cancer. Scale bars = 1 cm. C, D. Inhibition of ERK1/2 decreased liver weight (P < 0.01) and liver volume (P < 0.05). E. Top: Masson trichrome and immunohistochemical staining showed significant reductions of α-SMA, COL1A1, FN, and FAP expression. Corresponding dash lines indicated the tumor area of the liver lesions. Bottom: quantification of protein expression from five fields. Scale bars = 200 μm. *P < 0.05, **P < 0.01.

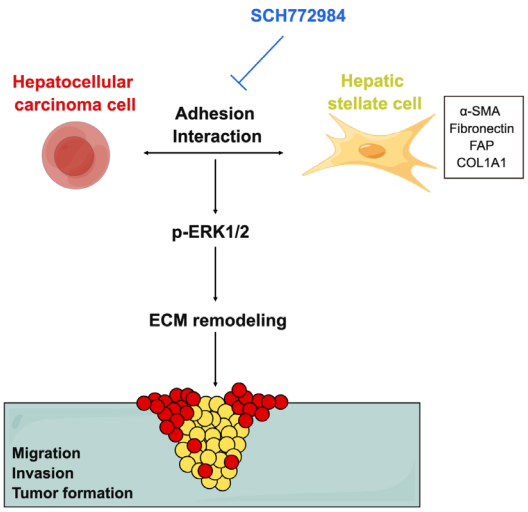

Figure 9. Schematic overview of ERK1/2 inhibition on HCC. Inhibition of ERK1/2 induces inactivation of HSCs by regulating α-SMA, Fibronectin, FAP and COL1A1. Inactivation of HSCs decreases tumor-stromal interactions and ECM production. As a result, inhibition of ERK1/2 suppresses invasiveness, migratory ability and tumor formation of HCC.

the TME of HCC. Additionally, CAFs were considered to originate from activated HSCs. Our RNA-seq results revealed that inactivation of ERK1/2 remarkably downregulated ECM-related signaling pathways in both cancer cells and stromal LX-2 cells. We analyzed and screened an ERK1/2 inhibition-related gene set, and the results revealed a significant correlation between ERK1/2 inhibition and CAF infiltration. Moreover, we verified that inactivation of ERK1/2 suppresses HCC tumor-stromal interactions and also inhibits the ECM production of both tumor cells and HSC LX-2 cells in vitro and in vivo. On the other hand, we confirmed that ERK1 and ERK2 are significantly correlated with the expression of FAP, FN1, and COL1A1 at the mRNA level by using TCGA HCC databases (Figure S4). However, how the ECM produced by tumor cells and HSCs regulates ECM remodeling in the TME is still unclear, and further investigation is needed.

This study demonstrates that ERK1/2 inactivation suppressed HCC tumor-stromal interactions and cancer progression by regulation of fibrosis and ECM remodeling. Our findings suggest ERK1/2 is a potential novel target for clinical therapy and further investigation is required.

Acknowledgements

We would like to acknowledge the help and support from the Bioinformatics Platform of Peking University Shenzhen Hospital (BI-PUSH). The authors thank the SRplot (http://www.bioinformatics.com.cn), an online platform for data analysis and visualization. We thank Dr. Gabrielle White Wolf from Liwen Bianji (Edanz) (www.liwenbianji.cn) for editing the English text of a draft of this manuscript. This research was supported by National Natural Science Foundation of China (82303436); Basic and Applied Basic Research Foundation of Guangdong Province Youth Fund Projects (2021A-1515110526); Shenzhen High-level Hospital Construction Fund; and Peking University Shenzhen Hospital Scientific Research Fund (KYQD2023242 and KYQD2022115).

Disclosure of conflict of interest

None.

Address correspondence to: Zilong Yan, Department of Hepatobiliary Surgery, Peking University Shenzhen Hospital, No. 1120 Lianhua Road, Futian District, Shenzhen 518000, Guangdong, China. Tel: +86-755-83923333 Ext. 2601; Fax: +86-755-839-23333; E-mail: 380785219@qq.com; yan0452@surg1.med.kyushu-u.ac.jp

References

[1] Yang JD, Hainaut P, Gores GJ, Amadou A, Plymoth A and Roberts LR. A global view of hepatocellular carcinoma: trends, risk, prevention and management. Nat Rev Gastroenterol Hepatol 2019; 16: 589-604.

[2] Crocetti L, Bargellini I and Cioni R. Loco-regional treatment of HCC: current status. Clin Radiol 2017; 72: 626-635.

[3] Zeng H, Chen W, Zheng R, Zhang S, Ji JS, Zou X, Xia C, Sun K, Yang Z, Li H, Wang N, Han R, Liu S, Li H, Mu H, He Y, Xu Y, Fu Z, Zhou Y, Jiang J, Yang Y, Chen J, Wei K, Fan D, Wang J, Fu F, Zhao D, Song G, Chen J, Jiang C, Zhou X, Gu X, Jin F, Li Q, Li Y, Wu T, Yan C, Dong J, Hua Z, Baade P, Bray F, Jemal A, Yu XQ and He J. Changing cancer survival in China during 2003-15: a pooled analysis of 17 population-based cancer registries. Lancet Glob Health 2018; 6: e555-e567.

[4] Marrero JA, Kulik LM, Sirlin CB, Zhu AX, Finn RS, Abecassis MM, Roberts LR and Heimbach JK. Diagnosis, staging, and management of hepatocellular carcinoma: 2018 practice guid-

ance by the American Association for the Study of Liver Diseases. Hepatology 2018; 68: 723-750.
[5] Fujiwara N, Friedman SL, Goossens N and Hoshida Y. Risk factors and prevention of hepatocellular carcinoma in the era of precision medicine. J Hepatol 2018; 68: 526-549.
[6] Hernandez-Gea V, Toffanin S, Friedman SL and Llovet JM. Role of the microenvironment in the pathogenesis and treatment of hepatocellular carcinoma. Gastroenterology 2013; 144: 512-527.
[7] Song M, He J, Pan QZ, Yang J, Zhao J, Zhang YJ, Huang Y, Tang Y, Wang Q, He J, Gu J, Li Y, Chen S, Zeng J, Zhou ZQ, Yang C, Han Y, Chen H, Xiang T, Weng DS and Xia JC. Cancer-associated fibroblast-mediated cellular crosstalk supports hepatocellular carcinoma progression. Hepatology 2021; 73: 1717-1735.
[8] Makino Y, Hikita H, Kodama T, Shigekawa M, Yamada R, Sakamori R, Eguchi H, Morii E, Yokoi H, Mukoyama M, Hiroshi S, Tatsumi T and Takehara T. CTGF mediates tumor-stroma interactions between hepatoma cells and hepatic stellate cells to accelerate HCC progression. Cancer Res 2018; 78: 4902-4914.
[9] Ji J, Eggert T, Budhu A, Forgues M, Takai A, Dang H, Ye Q, Lee JS, Kim JH, Greten TF and Wang XW. Hepatic stellate cell and monocyte interaction contributes to poor prognosis in hepatocellular carcinoma. Hepatology 2015; 62: 481-495.
[10] Yu G, Jing Y, Kou X, Ye F, Gao L, Fan Q, Yang Y, Zhao Q, Li R, Wu M and Wei L. Hepatic stellate cells secreted hepatocyte growth factor contributes to the chemoresistance of hepatocellular carcinoma. PLoS One 2013; 8: e73312.
[11] Liu J, Li P, Wang L, Li M, Ge Z, Noordam L, Lieshout R, Verstegen MMA, Ma B, Su J, Yang Q, Zhang R, Zhou G, Carrascosa LC, Sprengers D, IJzermans JNM, Smits R, Kwekkeboom J, van der Laan LJW, Peppelenbosch MP, Pan Q and Cao W. Cancer-associated fibroblasts provide a stromal niche for liver cancer organoids that confers trophic effects and therapy resistance. Cell Mol Gastroenterol Hepatol 2021; 11: 407-431.
[12] Yan Z, Da Q, Li Z, Lin Q, Yi J, Su Y, Yu G, Ren Q, Liu X, Lin Z, Qu J, Yin W and Liu J. Inhibition of NEK7 suppressed hepatocellular carcinoma progression by mediating cancer cell pyroptosis. Front Oncol 2022; 12: 812655.
[13] Sun B, Zhang X, Cheng X, Zhang Y, Chen L, Shi L, Liu Z, Qian H, Wu M and Yin Z. Intratumoral hepatic stellate cells as a poor prognostic marker and a new treatment target for hepatocellular carcinoma. PLoS One 2013; 8: e80212.
[14] Duran A, Hernandez ED, Reina-Campos M, Castilla EA, Subramaniam S, Raghunandan S, Roberts LR, Kisseleva T, Karin M, Diaz-Meco MT and Moscat J. p62/SQSTM1 by binding to vitamin D receptor inhibits hepatic stellate cell activity, fibrosis, and liver cancer. Cancer Cell 2016; 30: 595-609.
[15] Ullah R, Yin Q, Snell AH and Wan L. RAF-MEK-ERK pathway in cancer evolution and treatment. Semin Cancer Biol 2022; 85: 123-154.
[16] Bryant KL, Stalnecker CA, Zeitouni D, Klomp JE, Peng S, Tikunov AP, Gunda V, Pierobon M, Waters AM, George SD, Tomar G, Papke B, Hobbs GA, Yan L, Hayes TK, Diehl JN, Goode GD, Chaika NV, Wang Y, Zhang GF, Witkiewicz AK, Knudsen ES, Petricoin EF 3rd, Singh PK, Macdonald JM, Tran NL, Lyssiotis CA, Ying H, Kimmelman AC, Cox AD and Der CJ. Combination of ERK and autophagy inhibition as a treatment approach for pancreatic cancer. Nat Med 2019; 25: 628-640.
[17] Zou J, Lei T, Guo P, Yu J, Xu Q, Luo Y, Ke R and Huang D. Mechanisms shaping the role of ERK1/2 in cellular senescence (review). Mol Med Rep 2019; 19: 759-770.
[18] Xie YX, Liao R, Pan L and Du CY. ERK pathway activation contributes to the tumor-promoting effects of hepatic stellate cells in hepatocellular carcinoma. Immunol Lett 2017; 188: 116-123.
[19] Shang R, Song X, Wang P, Zhou Y, Lu X, Wang J, Xu M, Chen X, Utpatel K, Che L, Liang B, Cigliano A, Evert M, Calvisi DF and Chen X. Cabozantinib-based combination therapy for the treatment of hepatocellular carcinoma. Gut 2021; 70: 1746-1757.
[20] Xue C, Wang K, Jiang X, Gu C, Yu G, Zhong Y, Liu S, Nie Y, Zhou Y and Yang H. The down-regulation of SUZ12 accelerates the migration and invasion of liver cancer cells via activating ERK1/2 pathway. J Cancer 2019; 10: 1375-1384.
[21] Myojin Y, Hikita H, Sugiyama M, Sasaki Y, Fukumoto K, Sakane S, Makino Y, Takemura N, Yamada R, Shigekawa M, Kodama T, Sakamori R, Kobayashi S, Tatsumi T, Suemizu H, Eguchi H, Kokudo N, Mizokami M and Takehara T. Hepatic stellate cells in hepatocellular carcinoma promote tumor growth via growth differentiation factor 15 production. Gastroenterology 2021; 160: 1741-1754, e1716.
[22] Yan Z, Ohuchida K, Fei S, Zheng B, Guan W, Feng H, Kibe S, Ando Y, Koikawa K, Abe T, Iwamoto C, Shindo K, Moriyama T, Nakata K, Miyasaka Y, Ohtsuka T, Mizumoto K, Hashizume M and Nakamura M. Inhibition of ERK1/2 in cancer-associated pancreatic stellate cells suppresses cancer-stromal interaction and metastasis. J Exp Clin Cancer Res 2019; 38: 221.
[23] Yan Z, Ohuchida K, Zheng B, Okumura T, Takesue S, Nakayama H, Iwamoto C, Shindo K,

Moriyama T, Nakata K, Miyasaka Y, Ohtsuka T, Mizumoto K, Oda Y, Hashizume M and Nakamura M. CD110 promotes pancreatic cancer progression and its expression is correlated with poor prognosis. J Cancer Res Clin Oncol 2019; 145: 1147-1164.

[24] Uhlen M, Fagerberg L, Hallstrom BM, Lindskog C, Oksvold P, Mardinoglu A, Sivertsson A, Kampf C, Sjostedt E, Asplund A, Olsson I, Edlund K, Lundberg E, Navani S, Szigyarto CA, Odeberg J, Djureinovic D, Takanen JO, Hober S, Alm T, Edqvist PH, Berling H, Tegel H, Mulder J, Rockberg J, Nilsson P, Schwenk JM, Hamsten M, von Feilitzen K, Forsberg M, Persson L, Johansson F, Zwahlen M, von Heijne G, Nielsen J and Ponten F. Proteomics. Tissue-based map of the human proteome. Science 2015; 347: 1260419.

[25] Chandrashekar DS, Karthikeyan SK, Korla PK, Patel H, Shovon AR, Athar M, Netto GJ, Qin ZS, Kumar S, Manne U, Creighton CJ and Varambally S. UALCAN: an update to the integrated cancer data analysis platform. Neoplasia 2022; 25: 18-27.

[26] Li C, Tang Z, Zhang W, Ye Z and Liu F. GEPIA2021: integrating multiple deconvolution-based analysis into GEPIA. Nucleic Acids Res 2021; 49: W242-W246.

[27] Liu CJ, Hu FF, Xia MX, Han L, Zhang Q and Guo AY. GSCALite: a web server for gene set cancer analysis. Bioinformatics 2018; 34: 3771-3772.

[28] GTEx Consortium. The GTEx Consortium atlas of genetic regulatory effects across human tissues. Science 2020; 369: 1318-1330.

[29] Jia D, Li B, Wang JK, Wang P, Li CY, Lu LX, Tian WY, Yu XH, Zhang JC and Zheng Y. Expression and correlation of MIF and ERK1/2 in liver cirrhosis and hepatocellular carcinoma induced by hepatitis B. Pharmgenomics Pers Med 2023; 16: 381-388.

[30] Ogunwobi OO, Harricharran T, Huaman J, Galuza A, Odumuwagun O, Tan Y, Ma GX and Nguyen MT. Mechanisms of hepatocellular carcinoma progression. World J Gastroenterol 2019; 25: 2279-2293.

[31] Yang JD, Nakamura I and Roberts LR. The tumor microenvironment in hepatocellular carcinoma: current status and therapeutic targets. Semin Cancer Biol 2011; 21: 35-43.

[32] Amann T, Bataille F, Spruss T, Muhlbauer M, Gabele E, Scholmerich J, Kiefer P, Bosserhoff AK and Hellerbrand C. Activated hepatic stellate cells promote tumorigenicity of hepatocellular carcinoma. Cancer Sci 2009; 100: 646-653.

[33] Morris EJ, Jha S, Restaino CR, Dayananth P, Zhu H, Cooper A, Carr D, Deng Y, Jin W, Black S, Long B, Liu J, Dinunzio E, Windsor W, Zhang R, Zhao S, Angagaw MH, Pinheiro EM, Desai J, Xiao L, Shipps G, Hruza A, Wang J, Kelly J, Paliwal S, Gao X, Babu BS, Zhu L, Daublain P, Zhang L, Lutterbach BA, Pelletier MR, Philippar U, Siliphaivanh P, Witter D, Kirschmeier P, Bishop WR, Hicklin D, Gilliland DG, Jayaraman L, Zawel L, Fawell S and Samatar AA. Discovery of a novel ERK inhibitor with activity in models of acquired resistance to BRAF and MEK inhibitors. Cancer Discov 2013; 3: 742-750.

[34] Piguet AC, Majumder S, Maheshwari U, Manjunathan R, Saran U, Chatterjee S and Dufour JF. Everolimus is a potent inhibitor of activated hepatic stellate cell functions in vitro and in vivo, while demonstrating anti-angiogenic activities. Clin Sci (Lond) 2014; 126: 775-784.

[35] Tang Y. Curcumin targets multiple pathways to halt hepatic stellate cell activation: updated mechanisms in vitro and in vivo. Dig Dis Sci 2015; 60: 1554-1564.

[36] Fuchs BC, Hoshida Y, Fujii T, Wei L, Yamada S, Lauwers GY, McGinn CM, DePeralta DK, Chen X, Kuroda T, Lanuti M, Schmitt AD, Gupta S, Crenshaw A, Onofrio R, Taylor B, Winckler W, Bardeesy N, Caravan P, Golub TR and Tanabe KK. Epidermal growth factor receptor inhibition attenuates liver fibrosis and development of hepatocellular carcinoma. Hepatology 2014; 59: 1577-1590.

[37] Shimizu H, Tsubota T, Kanki K and Shiota G. All-trans retinoic acid ameliorates hepatic stellate cell activation via suppression of thioredoxin interacting protein expression. J Cell Physiol 2018; 233: 607-616.

[38] Baglieri J, Brenner DA and Kisseleva T. The role of fibrosis and liver-associated fibroblasts in the pathogenesis of hepatocellular carcinoma. Int J Mol Sci 2019; 20: 1723.

[39] Bataller R and Brenner DA. Liver fibrosis. J Clin Invest 2005; 115: 209-218.

[40] Wei SC and Yang J. Forcing through tumor metastasis: the interplay between tissue rigidity and epithelial-mesenchymal transition. Trends Cell Biol 2016; 26: 111-120.

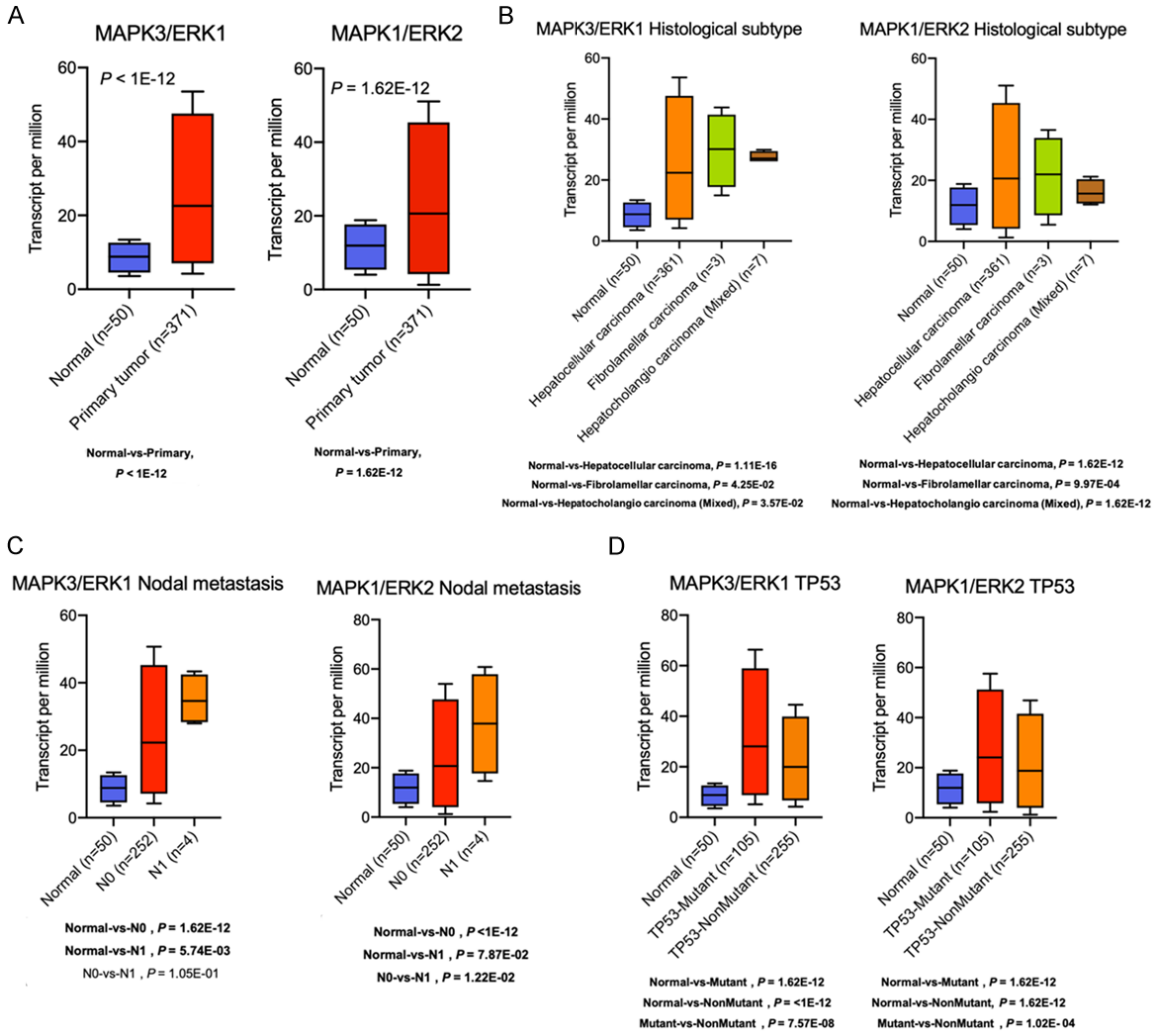

Figure S1. Correlations between ERK1/2 expression and clinicopathological characteristics by bioinformatics. A. Expressions of ERK1 and ERK2 were significantly upregulated in all types of liver tumor tissues (HCC, fibrolamellar carcinoma and hepatocholangial carcinoma) compared with tumor-adjacent normal tissues. B. Expressions of ERK1 and ERK2 in the indicated type of liver tumors compared with tumor-adjacent normal tissues. C. Expression of ERK1 and ERK2 in liver tumor in accordance with nodal metastasis. D. Expression of ERK1 and ERK2 in liver tumors in accordance with TP53 mutation.

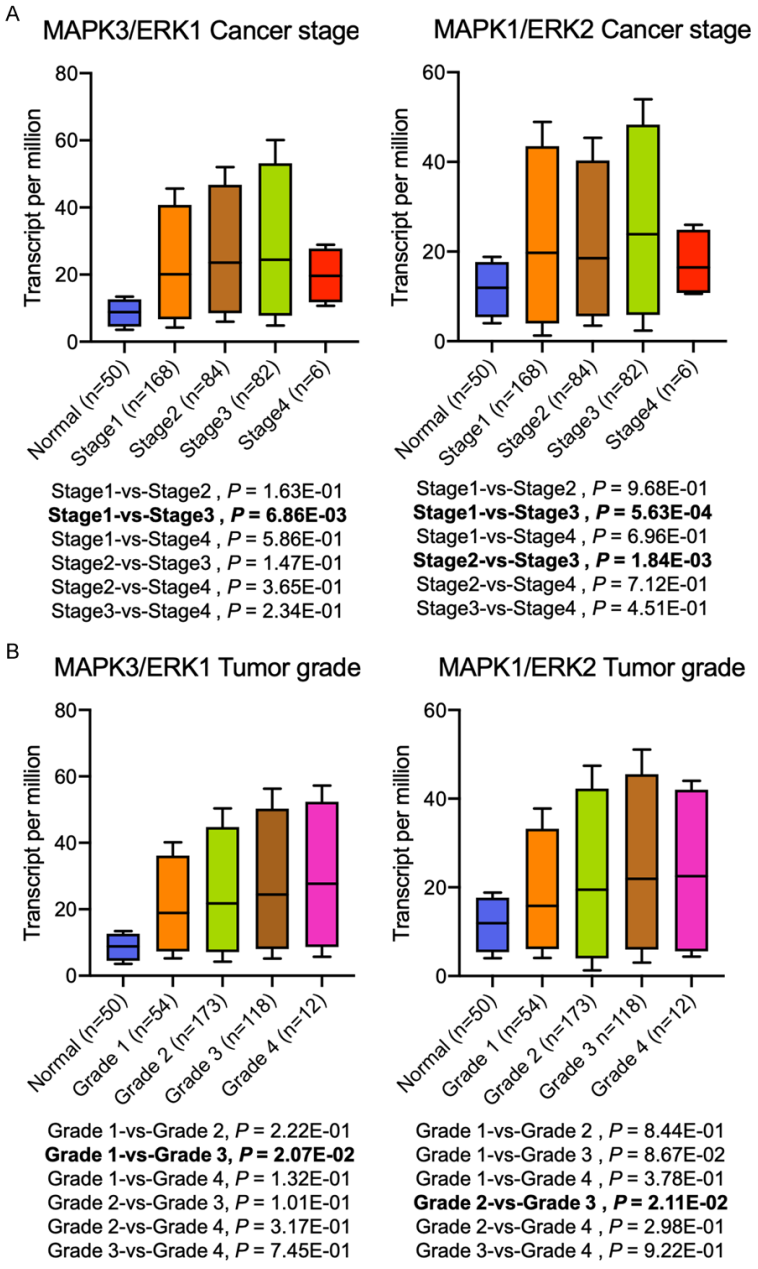

Figure S2. Expression of ERK1 and ERK2 in liver tumor in accordance with (A) cancer stage and (B) tumor grade.

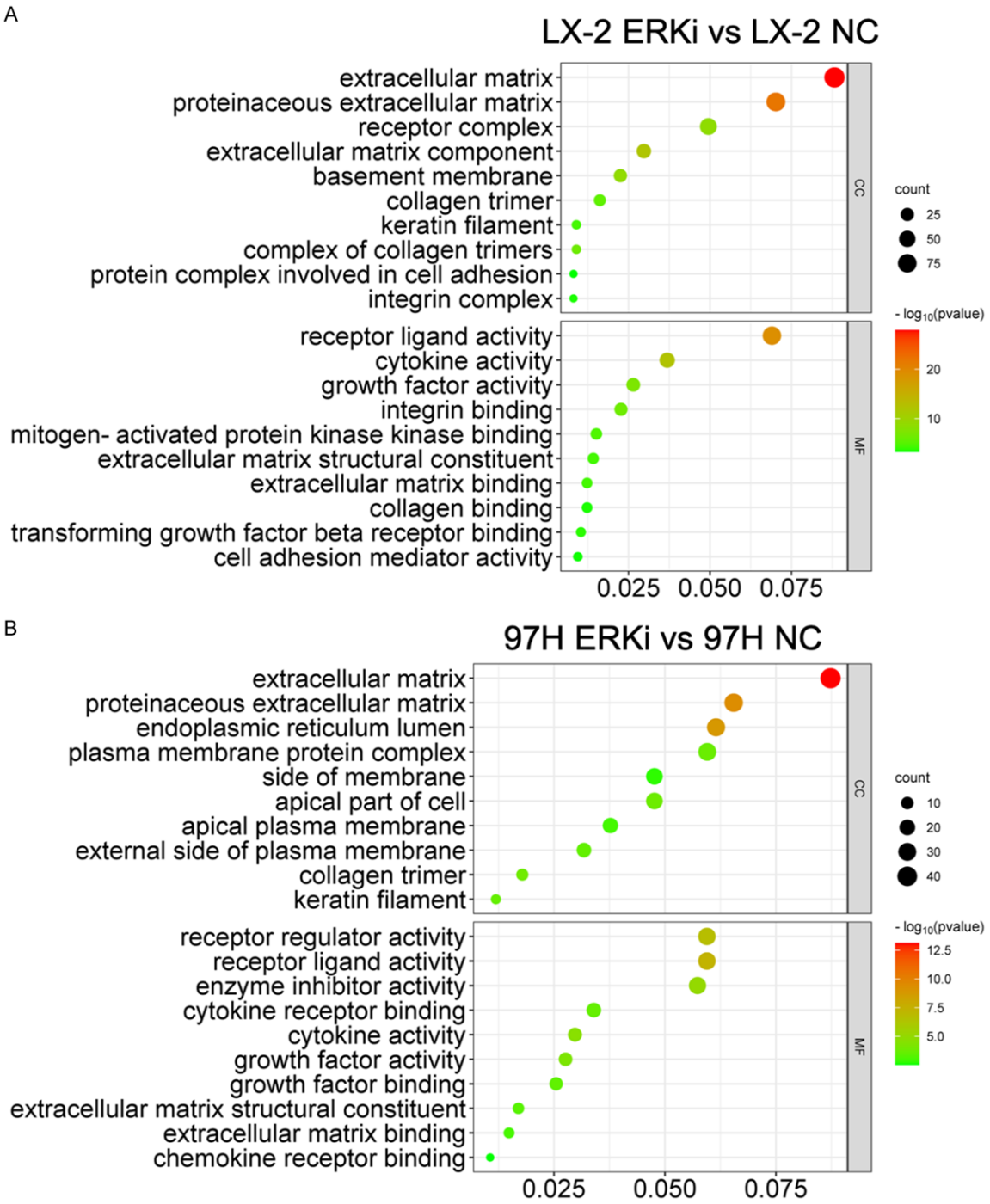

Figure S3. Cellular component and molecular function of Gene Ontology enrichment analyses. A, B. The cellular component and molecular function terms in aLX-2 cells and MHCC97H cells. The size of the dots represents the number of genes; a larger dot indicates a larger number of genes in the corresponding process.

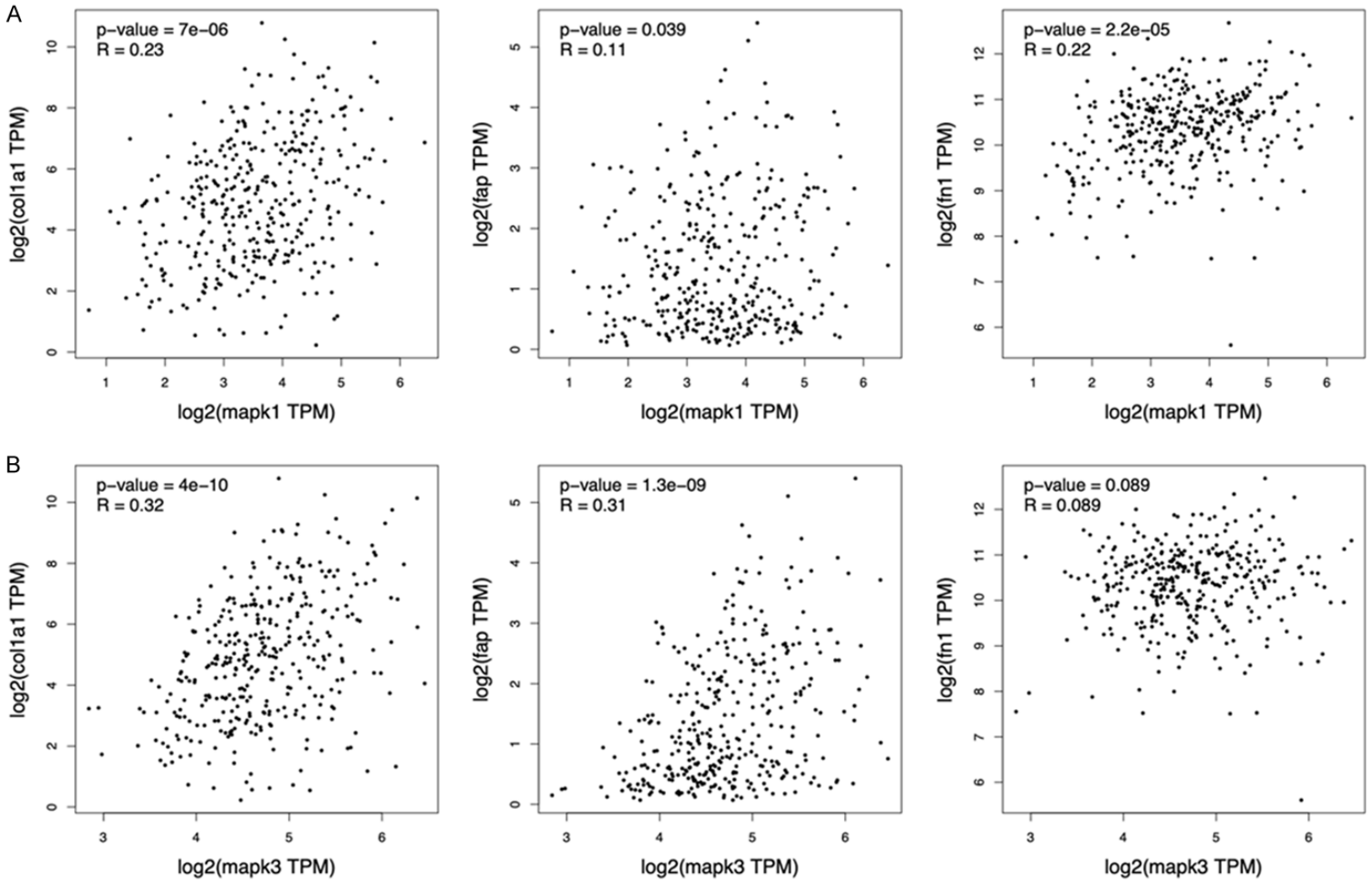

Figure S4. Correlation between COL1A1, FAP and FN1 with (A) ERK2 (MAPK1) or (B) ERK1 (MAPK3) at mRNA expression level.